NRC Publications Archive
Archives des publications du CNRC

Modeling and Optimization of the Hot Embossing Process for Micro and Nanocomponent Fabrication

Worgull, M.; Heckele, M.; Hétu, J. F.; Kabanemi, K.

This publication could be one of several versions: author's original, accepted manuscript or the publisher's version. / La version de cette publication peut être l'une des suivantes : la version prépublication de l'auteur, la version acceptée du manuscrit ou la version de l'éditeur.

For the publisher's version, please access the DOI link below./ Pour consulter la version de l'éditeur, utilisez le lien DOI ci-dessous.

NRC Publications Record / Notice d'Archives des publications de CNRC:
https://nrc-publications.canada.ca/eng/view/object/?id=0ccc2015-3d62-4bc5-8836-f4bf92c7b874
https://publications-cnrc.canada.ca/fra/voir/objet/?id=0ccc2015-3d62-4bc5-8836-f4bf92c7b874

Questions? Contact the NRC Publications Archive team at
PublicationsArchive-ArchivesPublications@nrc-cnrc.gc.ca. If you wish to email the authors directly, please see the first page of the publication for their contact information.

Vous avez des questions? Nous pouvons vous aider. Pour communiquer directement avec un auteur, consultez la première page de la revue dans laquelle son article a été publié afin de trouver ses coordonnées. Si vous n'arrivez pas à les repérer, communiquez avec nous à PublicationsArchive-ArchivesPublications@nrc-cnrc.gc.ca.

National Research Council Canada   Conseil national de recherches Canada

Canada

Modeling and optimization of the hot embossing process for micro- and nanocomponent fabrication

M. Worgull
M. Heckele
Forschungszentrum Karlsruhe
Institut für Mikrostrukturtechnik
Postfach 36 40
76021 Karlsruhe, Germany
E-mail: Matthias.Worgull@imt.fzk.de

J. F. Hétu
K. K. Kabanemi
National Research Council of Canada
Industrial Materials Institute
1500 Montreal Rd.
Ottowa, Ontario K1A 0R6
Canada

Abstract. Hot embossing and injection molding belong to the established plastic molding processes in microengineering. Based on experimental findings, a variety of microstructures have been replicated using these processes. However, with increasing requirements regarding the embossing surface, and the simultaneous decrease of the structure size down into the nanorange, increasing know-how is needed to adapt hot embossing to industrial standards. To reach this objective, a German-Canadian cooperation project has been launched to study hot embossing theoretically by process simulation and experimentally. The present publication reports on the proceeding and present first results. © 2006 Society of Photo-Optical Instrumentation Engineers. [DOI: 10.1117/1.2176729]

Subject terms: hot embossing; injection molding; plastic molding; nanocomponents.

1 Introduction

For the first time and independently of Ref. 1, embossing technology for replicating microstructures was applied by the Institute for Microstructure Technology of Forschungszentrum Karlsruhe in the early 1990s as part of the LIGA process.[2] In the course of further development, hot embossing has advanced to an independent process used apart from injection molding, injection embossing, and thermoforming. All processes mentioned have specific advantages. Consequently, they hardly compete with, but complement, each other, thus covering a wide spectrum of replicated microstructures.[3–5] Above all, process selection depends on the geometry of the microstructures and the surface to be patterned.

Injection molding is one of the economically most efficient processes. It is characterized by short cycle times and a high degree of automation. Mold filling is based on the injection of a melt into a closed cavity. Due to the existing gate systems and long flow paths, high shear stresses are generated during filling. Injection-molded components therefore possess comparatively high inner stresses. As a result of the long flow paths, filling of the cavities with extreme aspect ratios and the manufacture of large-area thin-walled components are aggravated on the microscale. To counteract this effect, the microstructures are fabricated in the variothermal mode.[6]

Injection compression molding assumes the position between injection molding and hot embossing, as it combines parts of both processes. Via a gap, a melt cake is injected into the tool. Then, the injection channel is sealed. The cavities are filled by a subsequent displacement- and force-controlled embossing process. Compared to injection molding, flow paths are reduced, and the manufacture of large-area thin-walled components is facilitated. One of the most popular examples is the manufacture of CDs. Cycle times in the order of a few seconds are state of the art.

Hot embossing is not based on an injection process, but uses semifinished products in the form of thin foils as the starting material for molding. The volume of the semifinished product is adapted to the surface area of the tool and height of the cavities. The advantage of the use of semifinished products is the homogeneous distribution of the melt directly over the complete surface area of the tool. Thus, cavities are filled with the shortest possible flow paths. A variothermal process conduct and small embossing rates result in comparatively small shear stresses, and hence, components with minimum stress. For this reason, hot embossing is predestined for large-area thin components and structures with extreme aspect ratios.[7] The modular design of a hot embossing facility ensures a relatively high degree of flexibility and short tool exchange times. It allows for the manufacture of a variety of structures from different materials. The process is suited for the fabrication of prototypes and small series.

Thermoforming also is an established process of plastic molding. One of the most popular examples is the manufacture of PET bottles by blow molding. This process may also be used for replicating microstructures.[8] Its advantage consists in the possibility of patterning thinnest polymer foils (about 2 μm) that cannot be processed by previous methods. In contrast to the earlier methods, molding takes place in the entropy-elastic state of a polymer rather than in the molten state.

All processes mentioned are based on the use of thermoplastic polymers as starting materials for the fabrication of microstructures. The only thing that differs is the type of material supply, which varies from granules to the use of semifinished products in the form of foils. Each process uses specific processing windows of the same polymer.

(a) Hot Embossing Process

Heating   Molding   Demolding
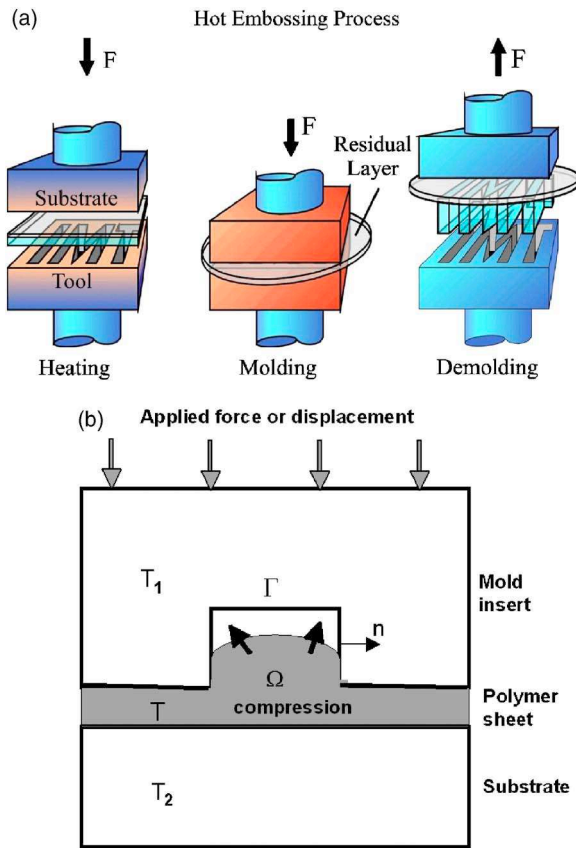
Fig. 1 (a) The hot embossing process: heating, molding, and demolding are the characteristic process steps. The hot embossing process is characterized by a residual layer, which allows for easy handling of the molded part, and (b) schematic view of the problem for mathematical description.

2 Hot Embossing

2.1 Process Steps

The hot embossing process is divided into four major steps:

1. heating of the semifinished product to molding temperature
2. isothermal molding by embossing (displacement controlled and force controlled)
3. cooling of the molded part to demolding temperature, with the force being maintained
4. demolding of the component by opening the tool.

One-sided embossing is represented schematically in Fig. 1.

Between the tool and substrate, a semifinished product, i.e., a polymer foil, is positioned. Thickness of the foil exceeds the structural height of the tool. The surface area of the foil covers the structured part of the tool. The tool and substrate are heated to the polymer molding temperature under vacuum. When the constant molding temperature is reached, embossing starts. At a constant embossing rate (on the order of 1 mm/min), tool and substrate are moved toward each other until the preset maximum embossing force is reached. Then, relative movement between the tool and substrate is controlled by the embossing force. The force is kept constant for an additional period (packing time, hold-

ing time), and the plastic material flows under constant force (packing pressure). At the same time, tool and substrate move further toward each other, while the thickness of the residual layer decreases with packing time. During this molding process, temperature remains constant. This isothermal embossing under vacuum is required to completely fill the cavities of the tool. Air inclusions or cooling during mold filling already may result in an incomplete molding of the microstructures, in particular at high aspect ratios. On the expiry of the packing time, cooling of the tool and substrate starts, while the embossing force is maintained. Cooling is continued until the temperature of the molded part drops below the glass transition temperature or melting point of the plastic. When the demolding temperature of the polymer is reached, the molded part is demolded from the tool by the opening movement, i.e., the relative movement between tool and substrate. Demolding only works in connection with an increased adhesion of the molded part on the substrate plate. Due to this adhesion, the demolding movement is transferred homogeneously and vertically to the molded part. Demolding is the most critical process step of hot embossing. Depending on the process parameters selected and the quality of the tool, demolding forces may vary by several factors. In extreme cases, demolding is no longer possible, and the structures are destroyed during demolding. Apart from the one-sided molding described, the process is also used for double-sided positioned embossing. The principle of the process remains the same. However, instead of the substrate, another tool is applied. To demold the molded part from one of both tool halves, special demolding mechanisms, such as ejector pins or pressurized-air demolding, are used. For a better understanding, the schematic representation of embossing in Fig. 1 is limited to the major process steps. Depending on the tool and polymer, the process and process parameters have to be adapted accordingly.

2.2 Process Parameters and Influencing Factors

In total, six groups of process parameters and factors influencing hot embossing can be distinguished. Process parameters and influencing factors can be distinguished by definition. Together, they influence the quality of the microstructured molded parts.[9]

Process parameters comprise those parameters that control the conduct of the hot embossing process. They include the molding temperature, embossing rate, embossing force, packing time, demolding temperature, and demolding rate. Another group consists of material parameters. They largely determine the process parameters. From the material parameters, processing windows are obtained, from which the process parameters result.

The six process parameters and material parameters are complemented by a number of influencing factors. Four categories of influencing factors can be distinguished.

- Tool: Evenness of the tool is of particular importance to ensure homogeneous thickness of the molded part over the complete embossing surface. Depending on the type of tool patterning, surface quality may vary, which determines the forces needed for demolding.
- Substrate: Like the tool, the substrate has to be extremely even over the complete surface area. Very im-
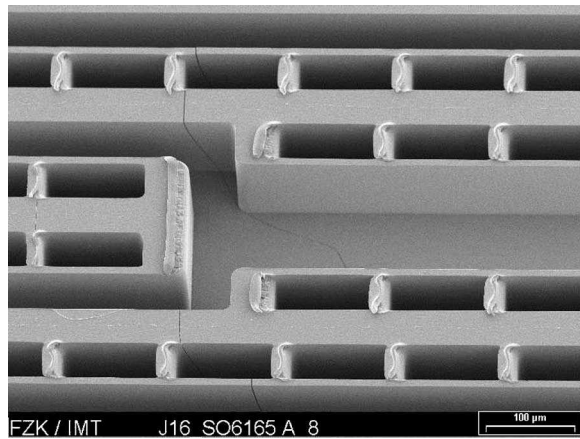
Fig. 2 Typical deformations of molded microstructures in the form of overdrawn edges. This type of deformation is caused during demolding by shrinkage differences between tool and polymer.

Fig. 3 In filigree components, there is the risk of individual structures or structural parts being torn off. This form of deformation is also caused at the beginning of demolding.

portant are favorable adhesion properties due to microstructured surfaces (e.g., lapping of the surface).
- Machine: Influences of hot embossing machines are manifold. Heat- and force-induced strains and distortions, positioning accuracy of traverses, and the precision of control have to be considered.
- Microstructures: The geometry, setup, and surface roughness of microstructures on the mold insert influence the demolding behavior. In particular, the steepness of the flanks of the microstructures and the aspect ratios are decisive criteria of demoldability.

Material parameters, process parameters, and influencing factors influence the quality of the molded microstructures.

2.3 Quality of Molded Parts and Sources of Deformation

Due to the variety of tool designs and customer requirements, the quality of molded parts has to be assessed individually. Irrespective of this, however, two criteria are of decisive importance, namely, contour accuracy and dimensional stability of the structures. Deviations from contour accuracy are defined by deformations that result from process control or mechanical defects of the tool, as illustrated in Figs. 2 and 3.

- Incomplete mold filling may be due to too little pressure or too small a temperature during embossing. In particular, structures with high aspect ratios and small cross sections may not be filled completely under certain circumstances. Rounded edges of the microstructures are characteristic of too little pressure.
- Sink marks are generated while cooling the molded parts. If the packing pressure is not sufficient to compensate temperature-induced shrinkage of the polymers, partial areas of increased shrinkage occur and detach from the tool wall.
- Distortions of microstructured or molded parts result from shrinkage differences in a molded part. Due to the pressure profile existing during embossing and the packing pressure phase, the peripheral areas of the molded part are subjected to less pressure. Shrinkage
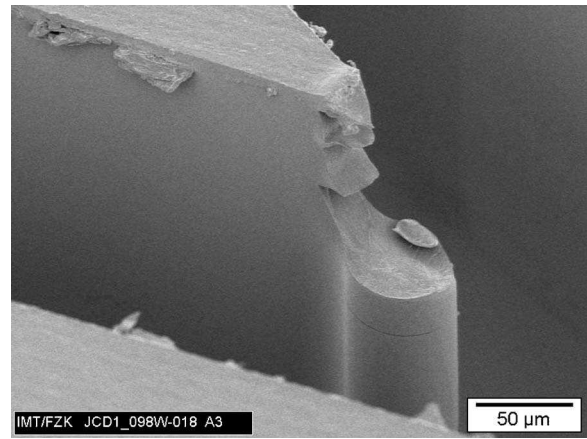
is pressure-dependent, such that shrinkage differences occur, which result in a distortion of the molded part.
- Overdrawn edges of structures are generated during demolding directly before the complete demolding of the structure. The shrinkage difference between polymer and tool results in forces that are directed to the center of the molded part. They may deform or destroy the upper edges of the microstructures.
- Overstretched and torn-off structures are also typical deformations caused during demolding. Due to friction and the contact stress resulting from the shrinkage difference between tool and polymer, tension forces act on the structures during demolding, which cause structures or parts of the structures to be overstretched or torn off, depending on their cross section. Undercuts drastically increase the risk of the structures being torn off.

3 Objective of the Project

So far, deformations have been reduced to a minimum by making use of the vast experience available. In the course of further development, however, there will be an increasing need for theoretically substantiated basic knowledge about the molding process.

Hot embossing may be analyzed theoretically by means of process simulation. Today, finite element method (FEM) simulation tools are state of the art in the field of plastic molding. However, no simulation tool exists that satisfactorily reproduces the entire process chain of hot embossing. Complete FEM modeling of a typical LIGA mold insert using PC-based FEM systems is not yet possible due to excessively high computational resources required to perform such analyses. Flow behavior of polymers during embossing has already been studied for a simple microstructure.[10,11] However, not only the individual freestanding microstructure is of interest, but also the structural field, and the type of arrangement of the individual microstructures. Modeling of structural fields allows statements to be made with respect to the arrangement and mutual influence of individual structures, and thus, a tool can be designed in advance.[9,12,13]

The joint project covered here is aimed at analyzing the individual process steps of hot embossing, understanding related effects, and deriving improvement potentials from the findings obtained for simple structured tools. Theoretical and practical analyses focus on the demolding process, as the risk of destroying microstructures is highest during this process step. Based on simulation models, parameter studies are performed, from which conclusions are drawn with respect to optimized process parameters, above all to reduce demolding forces.

The results of the simulation and accompanying experimental studies will pave the way for large-area embossing and the molding of nanostructures with high aspect ratios. These are requirements the hot embossing process will have to fulfill in the future.

4 Modeling and Simulation Tool

This section presents the mathematical model used for simulation of the decooling and demolding stages of the hot embossing process. First, we present the constitutive equations describing the thermoviscoelastic relaxation behavior of the polymer during the cooling and demolding stages. Then, we present contact and friction formulation used to simulate friction during the demolding phase. Finally, numerical algorithms as well as simulation results are presented.

4.1 Thermoviscoelastic Constitutive Equations

During the cooling of microstructures in the mold insert under an applied force, thermoviscoelastic stress calculations are performed according to the model developed by Kabanemi and Crochet.[7] We only briefly recall the basic assumptions of this model and refer the reader to the literature cited earlier.

The setting of the problem is as follows. A viscoelastic body at temperature T occupies the domain Ω, defined by the boundaries of the mold insert and the substrate, and is acted on by given forces, tractions, and thermal solicitations. A schematic view of the problem is shown in Fig. 1(b). We assume that a quasistatic process is valid. We further assume that during the hot embossing process, the polymer behaves as an isotropic thermorheologically simple material (see Refs. 14–16) in such a manner that stress components are related to histories of strain components and temperature through appropriate relaxation functions. The latter are derived from isothermal relaxation functions by assuming time-temperature equivalence on the basis of the WLF[17] equation. Relaxation of the specific volume is taken into account by introducing the concept of fictive temperature, i.e., the thermodynamic equilibrium temperature as a function of the polymer thermal history, introduced by Narayanaswamy.[18] The fictive temperature is calculated by introducing a volume relaxation function in the model. On that basis, one obtains the general form of the constitutive equations for thermorheologically simple materials.

Let us denote by s and s_{ij} the spherical and deviatoric components of the stress tensor σ, respectively, while e and e_{ij} denote the spherical and deviatoric components of the strain tensor ε, respectively. For an isotropic material, we use relaxation functions G_1 and G_2 in shear and dilatation, respectively, together with a modified time scale ξ. Hence, the stress-strain relation is expressed as:

$$s_{ij}(x,t) = \int_{-\infty}^{t} G_1(\xi - \xi') \frac{\partial e_{ij}(x,t')}{\partial t'} dt',\qquad(1)$$

$$s(x,t) = \int_{-\infty}^{t} G_2(\xi - \xi') \frac{\partial}{\partial t'}[e(x,t') - e_{th}(x,t')]dt'.\qquad(2)$$

The thermal strain e_{th} in Eq. (2) depends on the entire temperature history of the material point and not on the temperature at time t alone. The modified time scale ξ at a given point $\mathbf{x}(x,y,z)$ and at time t is given by

$$\xi(x,t) = \int_{0}^{t} \Phi[T(x,\lambda)]d\lambda.\qquad(3)$$

In Eq. (3), T is the temperature field and Φ the shift function often characterized by the WLF equation,[18] written as follows

$$\log \Phi = \frac{c_1(T - T_g)}{(c_2 + T - T_g)},\qquad(4)$$

where c_1 and c_2 are material constants and T_r is a reference temperature.

We wish to briefly comment on the relaxation functions G_1 and G_2 in Eqs. (1) and (2). Let 2μ and 3κ denote the value of G_1 and G_2 at time $t=0$, respectively. To simplify the system of equations, we assume that

$$G_1(t) = \frac{E}{1+v}\varphi(t) = 2\mu\varphi(t),\qquad(5)$$

$$G_2(t) = \frac{E}{1-2v}\varphi(t) = 3\kappa\varphi(t),\qquad(6)$$

where both G_1 and G_2 depend on the same relaxation function $\varphi(t)$. In Eqs. (5) and (6) E and v are Young's modulus and Poisson's ratio, respectively, and μ and κ are the shear modulus and the modulus of hydrostatic compression, respectively. We further decompose below the function $\varphi(t)$ as a sum of m exponentials, i.e.,

$$\varphi(t) = \sum_{r=1}^{m} g_r \exp(-t/\theta_r),\qquad(7)$$

in which θ_r is relaxation times and g_r material constants. The partial stress components s_{ij}^r and s^r associated with each relaxation time θ_r are given by

$$s_{ij} = \sum_{r=1}^{m} g_r s_{ij}^r,\qquad(8)$$

$$s = \sum_{r=1}^{m} g_r s^r. \tag{9}$$

During the cooling stage, it is convenient to represent the nonequilibrium behavior of the polymer, or its structural (volume) relaxation, in terms of two variables: the actual temperature T and a fictive or structural temperature T_f. We assume that, at initial time t_0, the initial temperature $T_f(\mathbf{x}, t_0) = T(\mathbf{x}, t_0)$ is above the glass transition temperature T_g, and that the specific volume $v(t_0)$ of the material is given. Following Narayanaswamy,[18] the specific volume $v(t)$ may be given by an integral equation of the type:

$$
\begin{aligned}
e_{th}(\mathbf{x}, t) &= \frac{1}{3} \frac{v(t) - v(t_0)}{v(t_0)} \\
&= \int_{T(\mathbf{x}, t_0)}^{T_f(\mathbf{x}, t)} \alpha_l(T') dT' + \int_{T_f(\mathbf{x}, t)}^{T(\mathbf{x}, t)} \alpha_g(T') dT',
\end{aligned} \tag{10}
$$

where α_l and α_g are the linear thermal expansion coefficients in the liquid and glassy states, respectively.

Finally, one needs a constitutive equation for the evolution of the fictive temperature T_f, for which we use the following model

$$T_f(\mathbf{x}, t) = T(\mathbf{x}, t) - \int_0^t M_v(\xi - \xi') \frac{\partial T(\mathbf{x}, t')}{\partial t'} dt', \tag{11}$$

where M_v is a volume relaxation function. In the liquid region, the relaxation is fast, and one obtains $T_f(\mathbf{x}, t) = T(\mathbf{x}, t)$. On the other hand, when the material is quenched below the glass transition temperature from temperature $T(t=0) = T_0$ above T_g, the relaxation does not exist and one obtains $T_f = T_0$. In this work, the same relaxation function is used for both M_v and φ.[19]

4.2 Contact and Friction Conditions

In the present formulation of the hot embossing process, it is assumed that the mold insert and the substrate behave as rigid bodies (see Fig. 1). We consider the case of an unilateral contact, which involves no penetration between the two bodies and is modeled with the Signorini conditions. We start our analysis by considering that a full contact zone Γ is developed at the entire interface between the polymer sheet and the mold insert. The first condition to satisfy is the nonpenetration condition. Let n be the interior normal to the mold insert that depends on the node under consideration. That normal can easily be obtained once the mold insert geometry is defined. Under these hypotheses, the nonpenetration boundary conditions on Γ can be written as

$$u_n \leq 0, \tag{12}$$

$$f_n \leq 0, \tag{13}$$

$$f_n \cdot u_n = 0. \tag{14}$$

Here, u_n is the normal displacement at the interface and f_n is the normal contact force. The first inequality, Eq. (12), represents the kinematic condition of no penetration of the

contact surface. The second inequality, Eq. (13), is the static condition of compressive or zero normal tractions. The third equation, Eq. (14), states that there is zero work done by the normal contact stress, i.e., the normal contact stresses exist only at the nodes where the polymer sheet is in contact with the rigid mold insert.

We model the frictional contact between the viscoelastic body and the mold insert with a Coulomb's law of dry friction, written as

$$|f_t| < \mu_s |f_n|. \tag{15}$$

Here, μ_s is a static friction coefficient associated with the stick friction constraint and f_t represents the tangential force on the contact boundary Γ. This static version of Coulomb's law states that the tangential shear cannot exceed the maximal frictional resistance. When the strict inequality $|f_t| < \mu_s |f_n|$ holds the surface of the polymer, it adheres to the mold insert and is in the so-called stick state, and when the inequality $|f_t| \geq \mu_s |f_n|$ holds, there is relative sliding, the so-called slip state. Coulomb's friction law is modified to include a dynamic friction coefficient μ_d associated with the slip condition when the static constraint is violated. In that case, the inequality $\mu_d \leq \mu_s$ holds. It follows from the previous analysis that the interface mold/polymer is divided into three zones, which are not known *a priori* and are part of the problem: stick, slip, and no contact or gap.

We use the penalty method to enforce contact constraints, and a regularization technique[20,21] to obtain estimates for the normal contact force f_n and the tangential frictional traction f_t as follows

$$f_n = -\lambda_n u_n, \tag{16}$$

$$f_t = -\lambda_t u_t, \tag{17}$$

where $\lambda_n > 0$ and $\lambda_t > 0$ are normal and tangential penalty parameters, respectively. The result is a solution to the contact problem that allows small violations of the contact constraints to estimate the direction and magnitude of the actual tractions.

It is a well-known fact that shrinkage that occurs during solidification of a polymer in a mold causes a gap between the two bodies. A sharp temperature drop occurs across that gap as a result of the thermal contact resistance. Although the gap is known as the air gap, in many instances, there is probably no air in it. In our numerical simulation, the thermal conductivity of the gap medium is taken as that of air. It is clear that the gap at the mold/part interface will reduce the cooling rate and increase the cooling time of the part. The gap computed at the interface mold/part is used in heat transfer calculations. The heat flux across the interface can be expressed as

$$q = -k \frac{\partial T}{\partial n} = \frac{k}{\Delta} (T_P - T_m), \tag{18}$$

where Δ is the gap distance, k is the thermal conductivity, and T_P and T_m are polymer and mold insert temperatures, respectively.
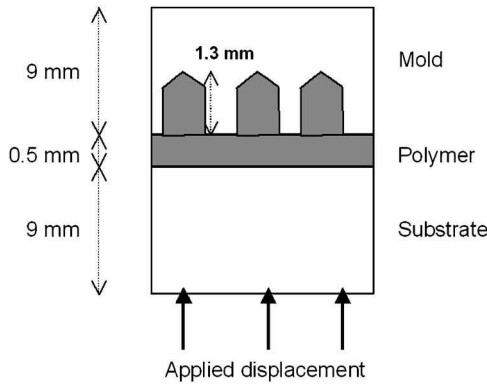
Fig. 4 Geometry of the mold insert.

Fig. 5 Applied stepwise displacement at the bottom side of the substrate during the process up to the moment of de-embossing.

With these assumptions, the mechanical problem of frictional contact of the viscoelastic body may be formulated as follows. Find a displacement vector **u**, and a stress field σ, such that

$$\nabla \cdot \sigma + \mathbf{f} = 0 \text{ in } \Omega,$$

$$u_n \leqslant 0, \quad f_n \leqslant 0, \quad f_n \cdot u_n = 0, \quad \text{on } \Gamma,$$

$$\text{with } |f_t| < \mu_s |f_n| \qquad u_t = 0,$$

$$|f_t| \geqslant \mu_s |f_n| \qquad \lambda_t > 0, \quad \text{such that } f_t = -\lambda_t u_t.$$

4.3 Solution Procedure for the Contact Problem

The proposed approach to solve the contact problem makes use of the procedure developed by Brunet.[21] In that procedure, the decision on whether a contact node is releasing or is in sticking or sliding condition is based on the total and relative magnitudes of updated contact forces. The condition is obtained as follows.

- If $f_n \geqslant 0$, the point is assumed to have experienced tension release, and in this case the penalty parameters and the normal and tangential contact force are set to zero.
- If $f_n < 0$ and $|f_t| < \mu_s |f_n|$, the node continues to stick and Eqs. (16) and (17) give appropriate estimations to the normal force and frictional traction. Sticking contact conditions must be assumed by setting the penalty parameters to a large positive number.
- If $f_n < 0$ and $|f_t| \geqslant \mu_s |f_n|$, then the state of the node must be updated to sliding with the consistent tangential penalty parameter $\lambda_t = \mu_d |f_n| / |u_t|$.

4.4 Numerical Results and Discussion

In this section, we apply the proposed method to the calculation of residual stresses and deformations of a typical microstructure, whose geometry and dimensions are shown in Fig. 4. The initial residual layer before the application of the normal force is 500 μm. The processing conditions are shown in Fig. 5, where a displacement is applied stepwise at the bottom side of the contact body. The applied force is
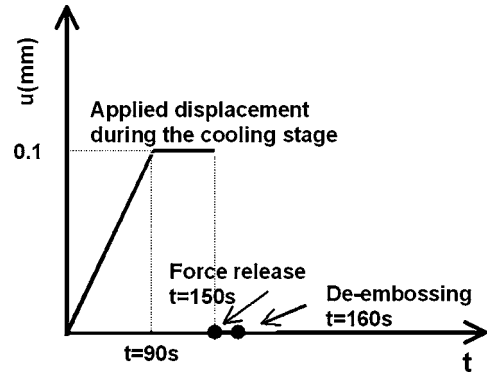
suddenly removed at $t = 150$ s. The polymer used is a polymethyl methacrylate (PMMA) (BASF Lucryl G77Q11), whose master curve at 110 °C is given later. The static μ_s and dynamic μ_d friction coefficients are 0.3 and 0.1, respectively. We have chosen a relaxation spectrum characterized by four relaxation times. To emphasize the effect of the applied force during cooling inside the mold insert, we first studied the behavior of a single microstructure during the embossing process. The shear stresses induced in the microstructure are shown in Fig. 6. High stresses are experienced around the re-entrant corner. These results also highlight the effect of contact friction on the deformation of the residual layer, which exhibits a nonuniform deformation when sliding occurs with friction. In fact, the part is cooling inside the mold, it is still under compression, and competition exists between the thermal shrinkage that tends to create a gap and the mechanical deformations induced by the applied force that tend to press the polymer against the mold to create contact, resulting in high stresses around corners. We then analyze the stresses and deformations induced in multiple microstructures. The normal displacement fields over the thickness, after 90 s of cooling and just before de-embossing, are shown in Fig. 7. Since the applied force has been removed after 150 s, the rate of deformation changes sign, and each microstructure returns more or less toward its initial shape, which depends on the embossing time, embossing temperature, and embossing pressure along with the viscoelasticity of the material. These results show the incomplete creep recovery experienced by the microstructures. The shear stress field after 90 s during cooling is shown in Fig. 8. These results correspond to the viscoelastic calculation with and without friction. As can be seen from these figures, microstructures in the central region behave almost in the same way, while those localized near boundaries exhibit high shear stresses. We also observe that residual stresses are localized around corners in all microstructures. These results have an incident on both the shape of microstructures and the quality of the replication. Figure 9 shows the gap formation at the interface of the microstructures and the mold insert after 40 s of cooling under an applied force and just before de-embossing. Since the applied force has been removed after 150 s, we observe a reformation of a very thin gap layer (about 3 μm) before de-embossing due to the creep recovery of the material.

(a)   (b)
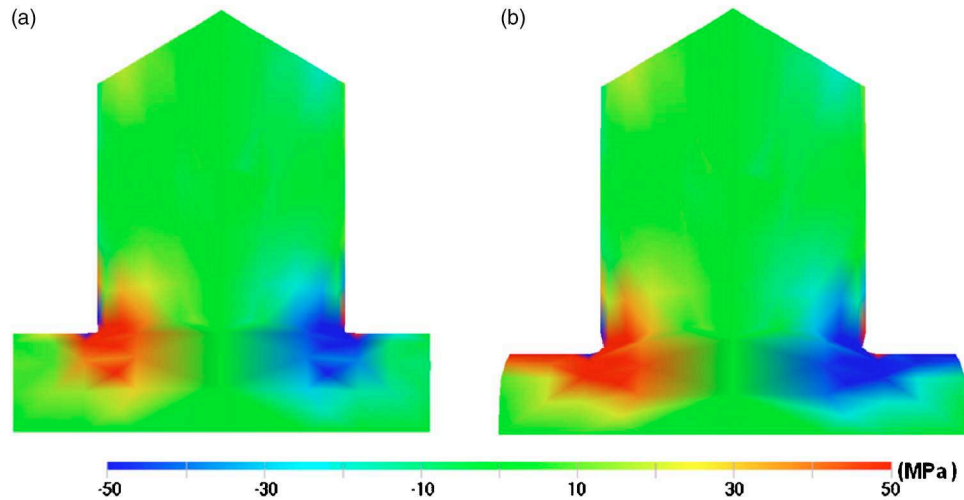
Fig. 6 Shear stresses in a cross section (t=90 s) during cooling of a single microstructure under an applied force: (a) without friction and (b) with friction.

5 Viscoelastic Material Model

5.1 *Creep Experiments*

The mechanical behavior of the glassy PMMA acrylic M-30 was investigated as function of stress and temperature by compression creep measurements in the vicinity of the glass transition temperature T_g, which is about 95°C. All the measurements were made on an Instron tensile tester. Thin flat samples of $10 \times 10 \times 3$ mm were cut from the PMMA sheet obtained by injection molding. Samples were compressed in the thin direction at two stress levels, i.e., 5 and 24 MPa, and then maintained constant for up to 30 min at various temperature levels of 80, 85, 90, 95, and 100°C. Our motivation for this experimental investigation was to simulate the hot embossing process in a tensile tester machine, and at the same time characterize creep viscoelastic properties near T_g that we believe, in conjunction with frictional contact between the polymer and the mold, may relate to the geometrical imperfection of embossed microstructures. The compressive stress-strain curves at various

temperature levels are shown in Fig. 10. At temperatures below T_g, deviations from linearity appear sooner. The stress-strain behavior is linear up to a compressive stress of about 3 MPa, which corresponds to a deformation of about 7%. Above that compressive stress, the material exhibits a nonlinear behavior characterized by a sharp increase of the stress. On the other hand, slightly above the glass transition temperature, i.e., around 95 to 100°C, the stress-strain behavior is linear up to roughly 5 MPa, corresponding to a deformation of about 40%, after which a sharp nonlinear increase of the stress is observed. We conclude from this finding that if the deformations in the embossing process of that PMMA are carried to a point where the viscoelastic behavior of the polymer becomes nonlinear, i.e., above 5 MPa at 100°C, then Eqs. (1) and (2) no longer hold. The creep behavior at two stress levels and various temperatures are shown in Figs. 11 and 12. As can be seen from these time profile figures, the equilibrium compliance in compression creep is not reached after a holding time of
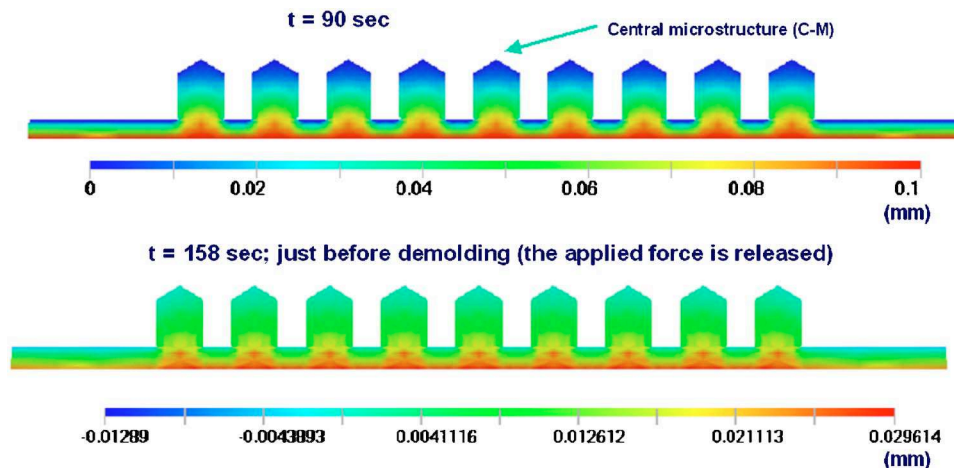
Fig. 7 Normal displacement field in a cross section at time t=90 s during cooling under an applied force and just before de-embossing (t =158 s), when the applied force is released.
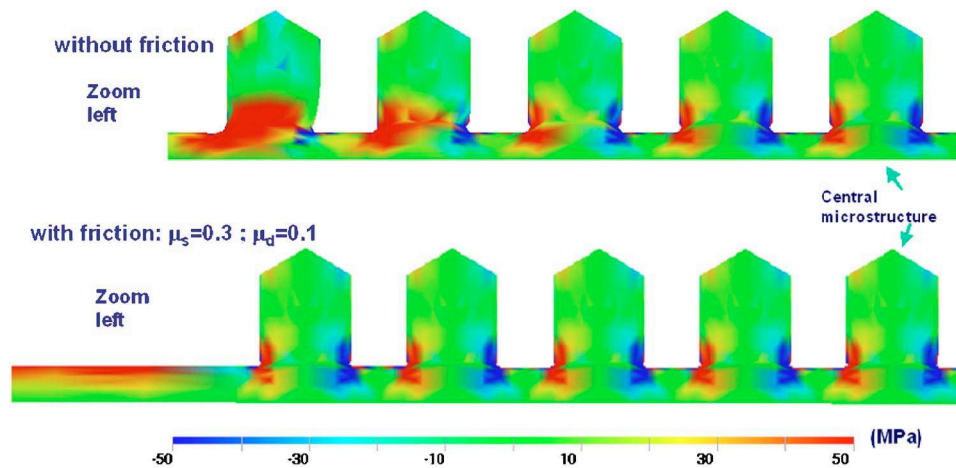
Fig. 8 Shear stresses in a cross section ($t=90$ s) during cooling under an applied force.

30 min. A reasonable appropriate range of processing conditions, i.e., embossing pressure, embossing temperature, and embossing time, can be deduced from the previous measurements.

5.2 Relaxation Experiments

Using the dynamic mechanical analysis (DMA), the temperature-dependent Young's modulus of PMMA G77Q11 was determined in a defined frequency range, i.e., under a time-depending bending load. Due to the equivalence of time (here, frequency) and temperature that is valid for polymers, the individual measurement curves of the temperature-dependent Young's modulus can be combined in a master curve by shifting along the time axis. The shift refers to a reference temperature, in our case, the glass temperature of $T_g=110\,°$C. The shifts resulted in the temperature-dependent shift factors and the constants C_1 and C_2 of the shift function. They are valid for the defined reference temperature only.

Based on a master curve and the corresponding shift function, Young's modulus can be determined as a function of time and temperature. The shape of the relaxation time curve remains unchanged. It is only shifted along the time axis. The shift principle is the basis of the material model for simulating the demolding behavior.

The time-and temperature-dependent Young's modulus is represented in Fig. 13. The shift function was interpolated to $T<100\,°$C for the temperature range of demolding being also covered by the simulation.

From Fig. 14, the relaxation behavior of PMMA G77Q11 can be estimated in comparison with typical process times of a hot embossing process. A relaxation worth mentioning can be observed from a temperature of about 170 °C. Within about 300 s, Young's modulus relaxes by an order of 10^4 Pa. With increasing temperature, relaxation times further decrease. At 180 °C, only 100 s are necessary, and at 200 °C, only 10 s. In contrast to this, relaxation time increases extremely with decreasing temperatures. At 160 °C, 1000 s are required; at 150 °C, about 2.8 h. Figure 11 shows that below a temperature of about 170 °C, relax-

ation times are too long for the stresses generated by molding being reduced largely. Molding temperatures should therefore be at least 170 °C or higher.

It is also evident from Fig. 14 that the master curve is not shifted linearly to the temperature. With decreasing temperature, the shift increases, which is due to the exponential behavior of the shift function. As a result, relaxation times do not increase linearly with smaller temperatures.

The measured time-temperature behavior of Young's modulus was approximated using a generalized Maxwell model with ten parameters according to Eq. (19).

$$E(t) = \sum_{i=1}^{n} E_i \cdot \exp\left(\frac{t}{\lambda_i}\right). \tag{19}$$

Figure 15 shows the master curve measured at 110 °C and the approximation solution by the Maxwell model. The description of the measurement curve with a ten-element model shows good agreement over 12 orders of magnitude.

5.3 Strength of the Material During Demolding

The temperature-dependent stress-strain characteristics were determined to derive the plastic deformation of structures, in particular the deformation resulting from demolding. For this purpose, tension rods were produced by hot embossing according to DIN EN ISO 527-2, with a view to obtain process-specific material properties of the tension rod. The tensile tests were carried out using a universal test machine of the type Instron 4505 in the temperature range typical of demolding from 60 to 100 °C. Apart from the temperature, typical demolding rates were considered by the tension rate being varied in the range of 0.5 to 10 mm/min. Based on the tension curves obtained, the yield stress was defined as the first stress value, at which strain is increased without increasing stress. The corresponding yield strain was in the range of about 4% for all temperatures studied. Figures 15 and 16 show the curves measured at typical demolding rates in the temperature range of 60 to 100 °C.

(a)

(b)
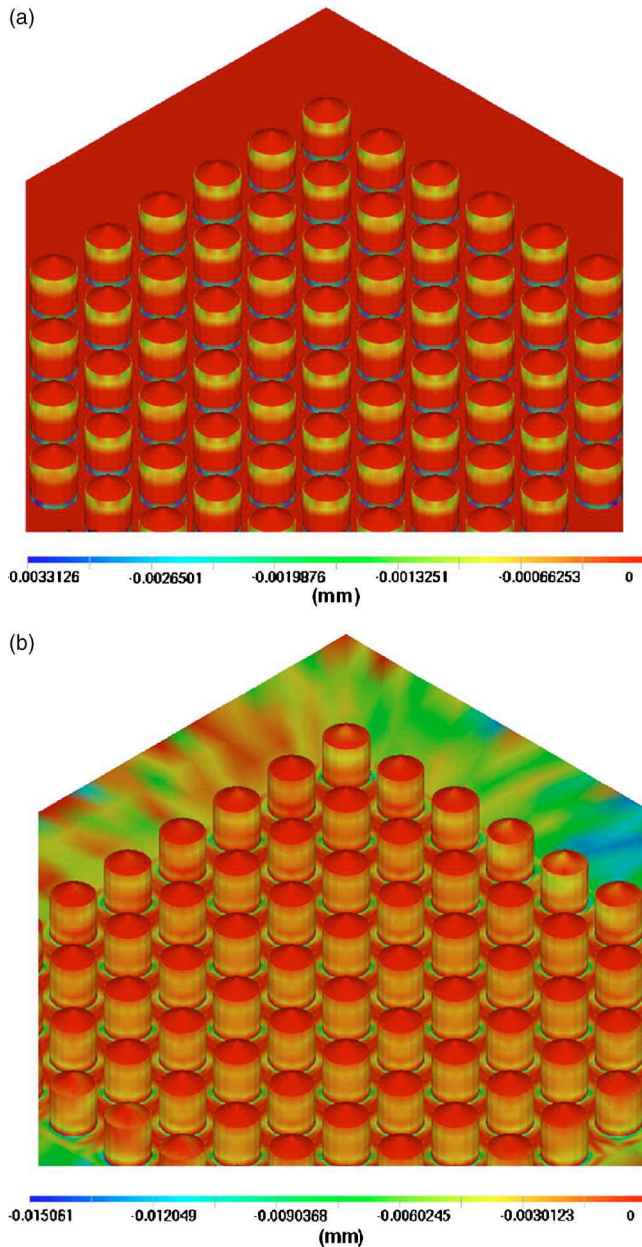
Fig. 9 (a) Gap formation during cooling under an applied force at $t=40$ s and (b) gap reformation just before de-embossing at $t=158$ s.

Fig. 10 Stress-strain curves at various temperature levels in compression tests for the PMMA Acrylic M-30.

5.4 Measurement of Friction Behavior

The problem of demolding microstructures gains importance with the increasing size of the embossing surface and smaller structures. Thus, central task of the project described here is the development of a measurement method by means of which static and dynamic friction can be determined during demolding under typical hot embossing conditions. Static and dynamic friction forces in microstructured tools, however, can only be measured as the sum in the form of demolding forces. Detailed analysis fails, as it is impossible to determine the normal forces acting on the individual sidewalls of the structured tool, which largely depend on the shrinkage of the component, and, thus, on a multitude of process parameters and influencing factors.
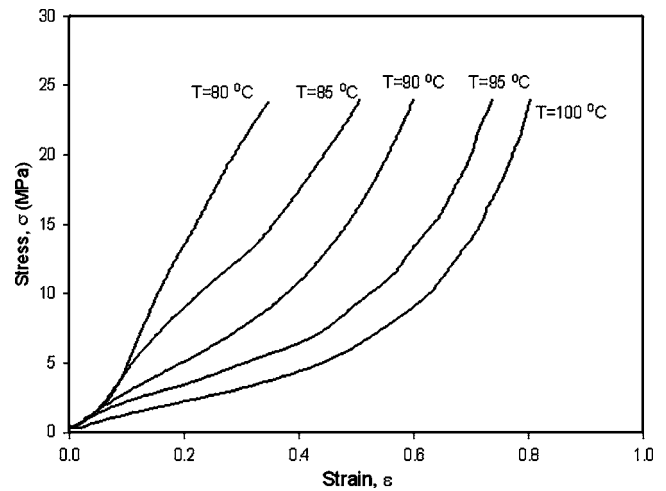
Moreover, force measurement systems of high spatial resolution, which might be integrated in the microstructured tool, are lacking. For this reason, static and dynamic friction forces were measured using a macroscopic measurement system. The approach to determining friction coefficients according to DIN/ISO is not suitable, as the boundary conditions defined in these standards do not reflect those of the hot embossing process. Within the framework of the project described here, a measurement process has been developed that includes an embossing process prior to the measurement of static and dynamic friction forces. Apart from the surface roughness of the specimen and the defined adjustable normal force, the influence of the process parameters of hot embossing, i.e., embossing pressure, embossing temperature, demolding temperature, and demolding rate, on the demolding force is considered (Fig. 17).

As far as material and surface roughness are concerned, the specimens used represent typical values of microstructured tools. Both the surface roughness of tools produced
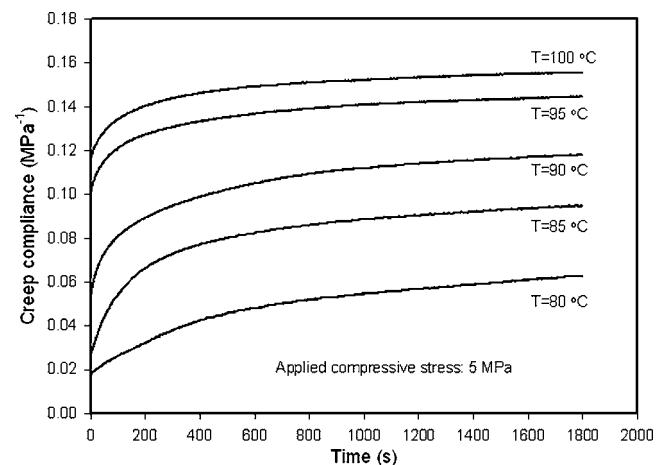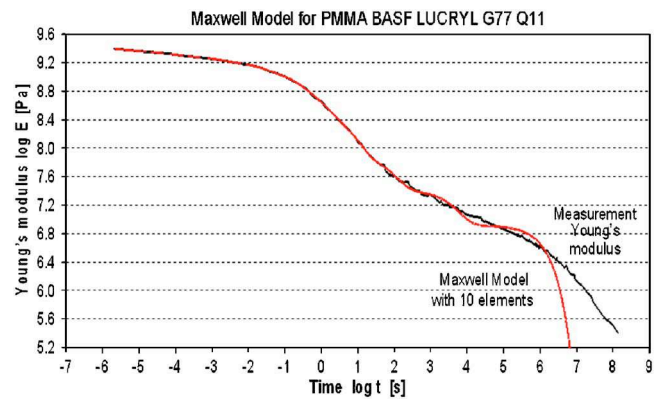

Fig. 11 Creep compliance curves at various temperature levels in compression tests for the PMMA Acrylic M3-0. The applied compressive stress is 5 MPa.
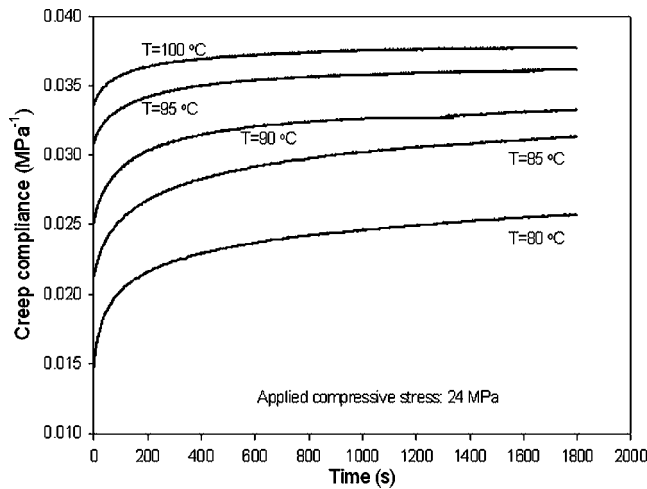
Fig. 12 Creep compliance curves at various temperature levels in compression tests for the PMMA Acrylic M-30. The applied compressive stress is 24 MPa.


Fig. 14 Approximation of the time-temperature behavior of Young's modulus by a generalized Maxwell model with ten elements. Over a time range of 12 orders of magnitude, good agreement is reached between measurement and model.

by electroplating and those of tools manufactured by micromechanical processes are considered. The advantage of this measurement method is that the history of the plastic, namely, the embossing process, is taken into account. Furthermore, the individual parameters influencing the demolding force can be assessed systematically.

Two characteristic measurement curves of the high number of measurements are shown in Fig. 18. The breaking away of the structures at the beginning of demolding is of decisive importance to demolding the microstructures, as the highest forces are encountered at this moment. This point is specified by static friction. In contrast to dynamic friction, static friction is defined clearly by the peak of the measurement curve. After the plastic has broken away from
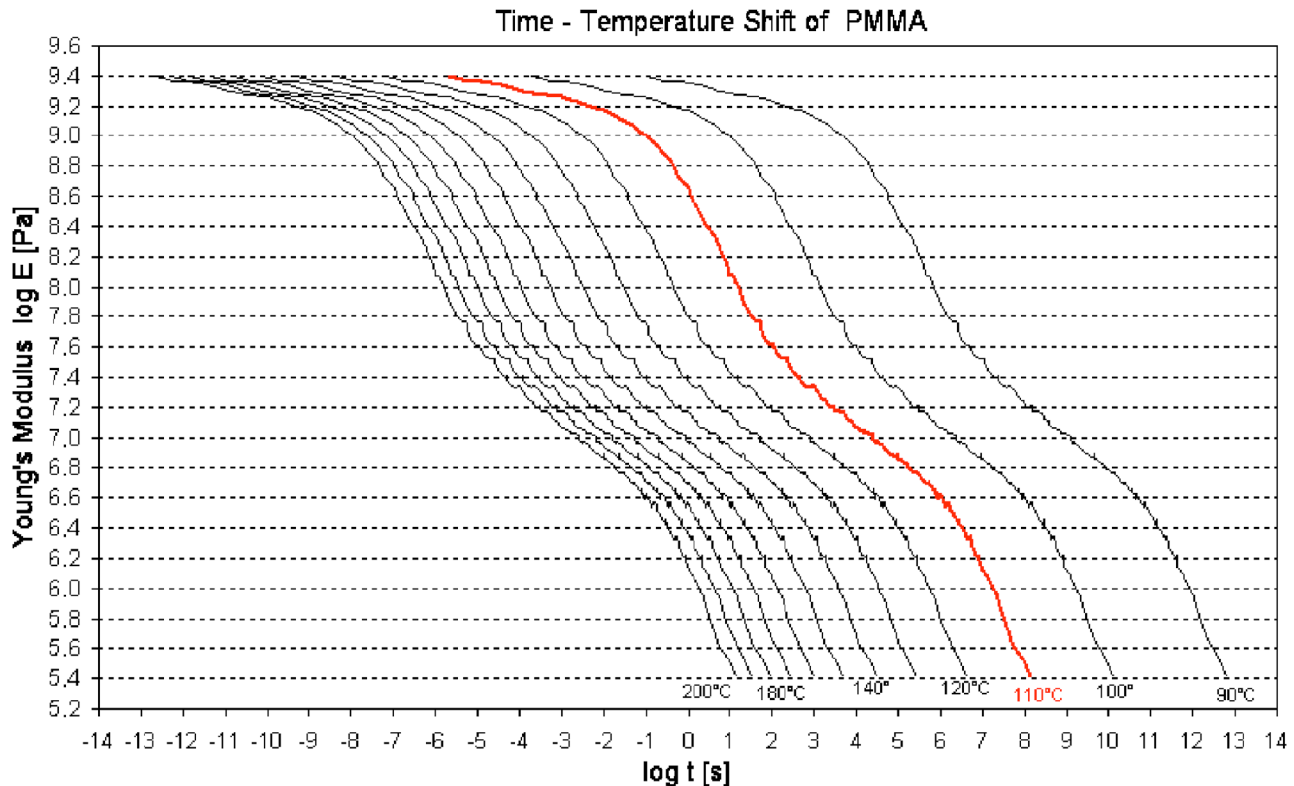
Fig. 13 Time- and temperature-dependent Young's modulus measured for PMMA Lucryl G77Q11. The decrease in Young's modulus is attributed to relaxation processes. From a temperature of about 170°C, the relaxation times are in the range of typical process times. Above this temperature, stress reduction by relaxation processes has to be expected in embossed components. Below the temperature of 170°C, relaxation times exceed typical process times. Therefore, stresses in the molded part are reduced to a far smaller degree.
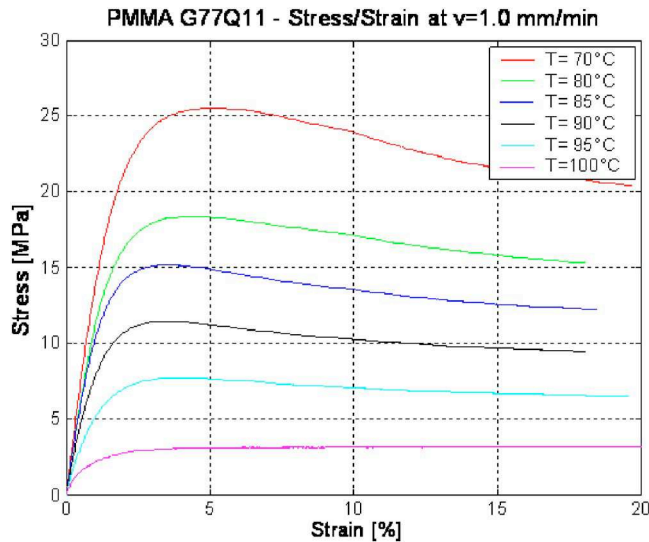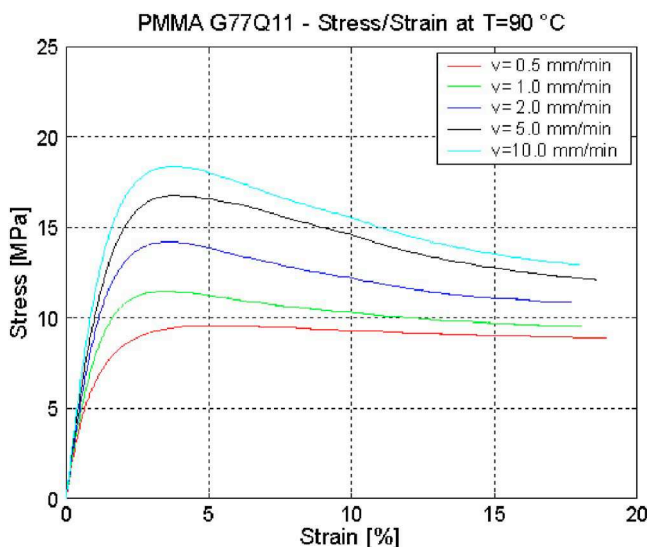
Fig. 15 Stress-strain curves measured as a function of temperature at a constant tension rate of 1 mm/min. The strength of the plastic decreases drastically with increasing temperature. For defect-free demolding, an adapted demolding temperature has to be selected, which is as close as possible to the glass transition temperature, but ensures sufficient strength to prevent the component from being destroyed.
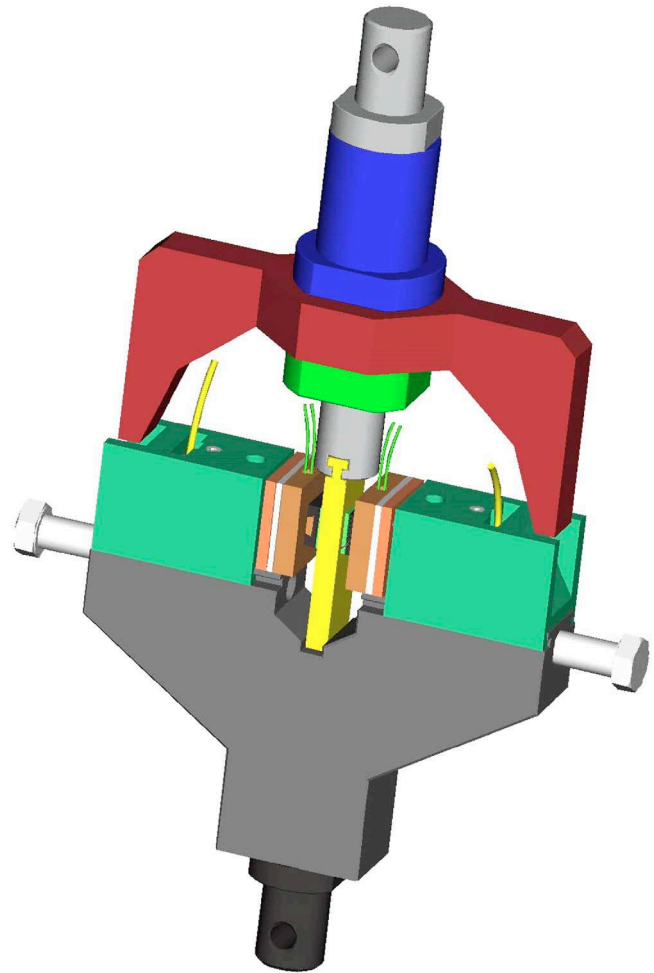
the tool, further demolding is characterized by sliding along the vertical sidewalls. Dynamic friction is reflected by the slip-stick effect, as evident from Fig. 16. The results obtained in the form of static and dynamic friction coefficients are used for the modeling of hot embossing.

## 6 Microstructure/Nanostructure Interface

Simulation of the hot embossing process is not only based on existing microstructures, but considers also the future applications of nanotechnology. It is therefore necessary to


Fig. 17 Test arrangement to determine adhesion and friction under typical hot embossing conditions. The test arrangement can be used in a tension machine. The advantage of the arrangement is an integrated molding cycle before the measurement of friction is started.

Fig. 16 Stress-strain curves measured as a function of the tension rate at a constant temperature of 90°C. The strength of the plastic is increased with increasing tension rate due to the viscoelastic behavior.
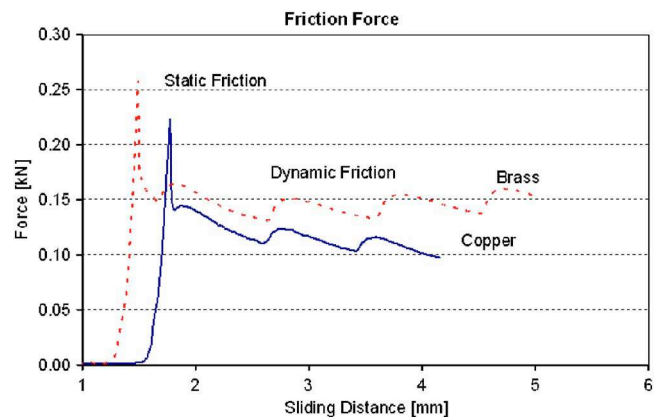

Fig. 18 Friction force measured between the molded polymer and a brass and a copper surface. Because of the integrated molding cycle, static and dynamic friction force can be measured under typical demolding conditions. With the measurement arrangement, friction coefficients can be calculated for different material combinations.
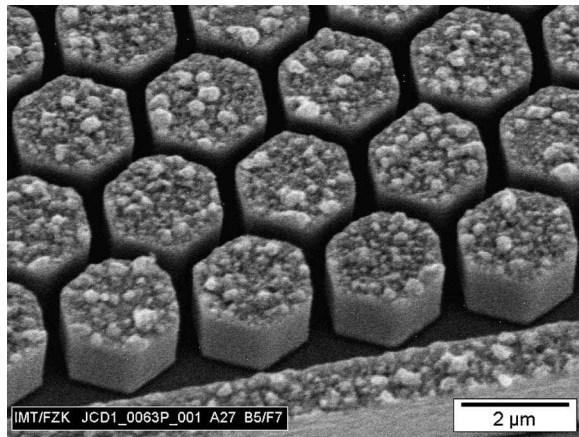
Fig. 19 Detail of a nanostructured nickel shim mold. The mold is fabricated by E-beam lithography and electroplating. The structure height is 2 μm, the gap is in the range of 0.6 μm.
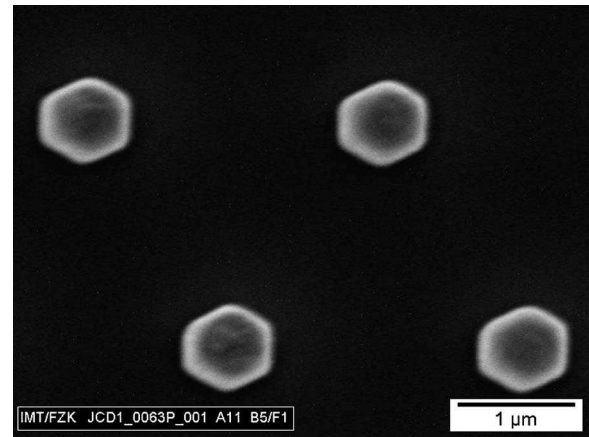
Fig. 20 Detail of a nanostructured nickel shim mold with honeycomb structures. The structure height is 2 μm and the diameter of the structures is in the range of 0.5 μm.

extend simulation to also cover structural sizes in the range between nanostructures and microstructures.

The border between nanostructures and microstructures is not defined unambiguously. Nanostructures produced by nanoimprinting normally do not possess any extreme aspect ratios. The aspect ratio is on the order of 1. In contrast to this, microstructures with extreme aspect ratios in excess of 50 may be produced by certain fabrication methods. Replication of such structures requires a high degree of understanding of the process. Between both structural dimensions, nanostructures with relatively small aspect ratios and microstructures that can be replicated with high aspect ratios, there is a gap. This is the range of the so-called submicrostructures, i.e., structures in the range of ≤ 1 μm with an aspect ratio far beyond 1. In this range, a number of applications can be found, for example, micro-/nanofluidics and photonic crystals.

The project presented here is aimed at producing and simulating the replication of submicrostructures. When producing submicrostructures, replication by hot embossing has the advantages of short flow paths, resulting low-stress components, and the possibility of producing large-area structured fields. In the course of the project, submicrostructures with varying aspect ratios were produced and replicated by hot embossing.

6.1 *Manufacture of Submicrostructures*

To demonstrate the molding of submicrostructures, honeycomb structures were exposed in a 2-μm-high resist by electron-beam lithography. The fields structured were 100 $\times$ 100 μm^2 in size. The individual fields contained honeycomb structures with varying distances and widths across flats, such that the spectrum of aspect ratios ranged from about 1 to 4. From the exposed resist, a 4-in. Ni shim molding tool was produced by electroplating (Figs. 19 and 20).

Replication in plastic represents a challenge, as the influence of plastic shrinkage in relation to the structure height increases during cooling and demolding. Due to the filigree structures, the risk of destroying the structures during demolding increases as well, especially for large-area

structured fields. To minimize shrinkage, design measure such as a holding unit of the Ni shim tool, as well as the integration of auxiliary structures, are feasible. Auxiliary structures in particular reduce shrinkage and protect the filigree submicrostructures against high transverse forces that may cause defects of these structures during demolding. Filling of the microcavities is ensured by the vacuum and an appropriate process conduct. Incomplete filling of the mold was not observed. The demolding forces measured are <4 N for the complete structured surface. As a rule, the structures were demolded without destruction, although the influence of shrinkage could not be eliminated completely. This was particularly obvious for structures with a small width across flat and a large web width. Here, shrinkage was found to be on the order of the structure (about 0.5 μm), such that sheared edges occurred.

Structures with an aspect ratio of about 3.5 were molded at a web width of the honeycomb structures of about 0.6 μm (Figs. 21 and 22).

While the structured embossing surface area of 100 $\times$ 100 μm^2 was very small, a far larger field was structured in a second step to analyze the influence of the structured surface area on the demolding behavior. This design is
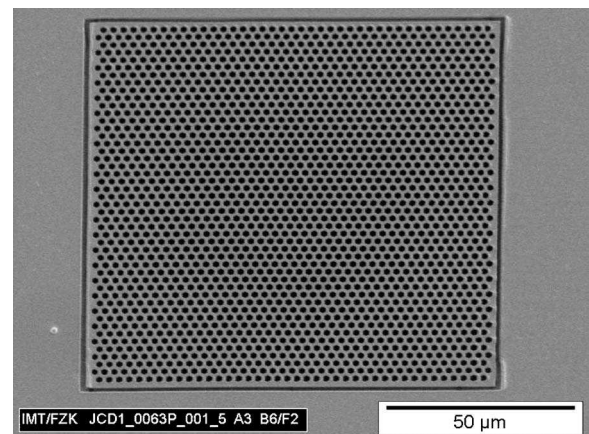
Fig. 21 Molded area of 100$\times$100 μm^2.
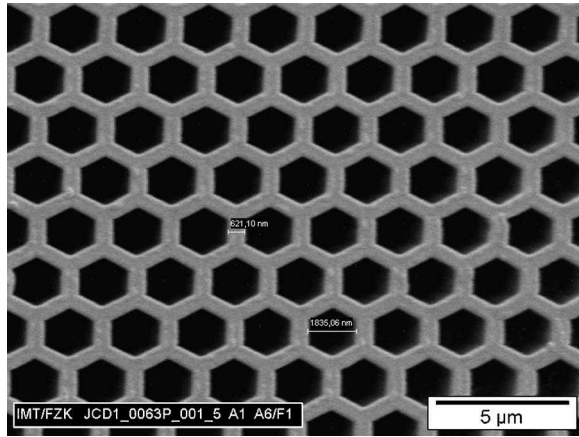
Fig. 22 Detail of a nanostructured molded part with an aspect ratio of 3.5. The design of this honeycomb structure in the nanorange is also used for a verification of the simulation results.

modeled in parallel by the National Research Council of Canada and serves as a basis of simulations, the results of which will be compared with the experimental results.

7 Conclusion

To meet future requirements in terms of an increasing embossing surface area and a simultaneously decreasing structure size, a German-Canadian cooperation project has been initiated between Forschungszentrum Karlsruhe (FZK) and the National Research Council Canada (NRC) to systematically analyze the hot embossing process for the replication of microstructures. Using selected microstructured tools, the process is modeled, and the simulation results are compared with practical experiments.

For simulation, a typical representative of a thermoplastic material is analyzed in detail by NRC with respect to its behavior during molding. Based on this analysis, a viscoelastic material model is developed. Moreover, the influence of adhesion and friction is accounted for when simulating the demolding behavior. Systematic measurement of adhesion and friction coefficients under typical process conditions is another major part of the project. In addition to the analysis of hot embossing for classical microstructures, particular attention is paid to the range between nanostructures and microstructures. In this range of so-called submicrostructures with high aspect ratios, tools are produced by electron-beam lithography and electroplating. On this basis, simulations and experiments will be performed.

References

1. M. T. Gale, J. Kane, and K. Knop, "ZOD images: Embossable surface-relief structures for color and black-and-White reproduction," *J. Appl. Photogr. Eng.* **4**, 41 (1978).
2. A. Michel, R. Ruprecht, M. Harmening, and W. Bacher, "Abformung von mikrostrukturen auf prozessierten wafern" KfK Bericht 5171, Dissertation A. Michel, Universität Karlsruhe, Institut für Mikrostrukturtechnik (1993).
3. T. Hanemann, M. Heckele, and V. Piotter, "Current status of micromolding technology," *Polym. News* **25**, 224–229 (2000).
4. M. Heckele and W. K. Schomburg, "Review on micro molding of thermoplastic polymers," *J. Micromech. Microeng.* **14**, R1–R14 (2004).
5. M. Heckele, W. Bacher, T. Hanemann, and H. Ulrich, "Hot embossing and injection molding for microoptical components," *Proc. SPIE* **3135**, 24–29 (1997).
6. T. Benzler, V. Piotter, T. Hanemann, K. Mueller, P. Norajitra, R. Ruprecht, and J. Hausselt, "Innovations in molding technologies for microfabrication," *Proc. SPIE* **3874**, 53–60 (1999).
7. K. K. Kabanemi and M. J. Crochet, "Thermoviscoelastic calculation of residual stresses and residual shapes of injection molded parts," *Int. Polym. Process.* **1**, 60 (1992).
8. R. Truckenmüller, "Herstellung dreidimensionaler mikrostrukturen aus polymermembranen," Dissertation R. Truckenmüller, Universität Karlsruhe, Institut für Mikrostrukturtechnik (2002).
9. M. Worgull, M. Heckele, and W. K. Schomburg, "Analysis of the micro hot embossing process," Forschungszentrum Karlsruhe, FZKA-Bericht 6922.
10. Y. Juang, L. J. Lee, and K. W. Koelling, "Hot embossing in microfabrication. Part 1: Experimental," *Polym. Eng. Sci.* **42**(3), 539–550 (2002).
11. Y. Juang, L. J. Lee, and K. W. Koelling, "Hot embossing in microfabrication. Part 2: Rheological characterization and process analysis," *Polym. Eng. Sci.* **42**(3), 551–556 (2002).
12. M. Worgull and M. Heckele, "New aspects of simulation in hot embossing," *Microsyst. Technol.* **10**, 432–437 (2004).
13. M. Worgull, M. Heckele, and W. Schomburg, "Large scale hot embossing," DTIP Conf. 2004, Montreux.
14. A. I. Isayev, *Injection and Compression Molding Fundamentals*, Marcel Dekker, New York (1987).
15. L. C. E. Struik, *Internal Stresses, Dimensional Instabilities and Molecular Orientations in Plastics*, Wiley and Sons, New York (1990).
16. J. D. Ferry, *Mechanical Properties of Polymers*, 2nd ed., Wiley and Sons, New York (1970).
17. M. L. Williams, R. F. Landel, and J. D. Ferry, *J. Am. Chem. Soc.* **77**, 3701 (1955).
18. O. S. Narayanaswamy, "A model of structural relaxation in glass," *J. Am. Ceram. Soc.* **54**, 491 (1971).
19. A. J. Kovacs, "La contraction isotherme du volume des polymères amorphes," *J. Polym. Sci.* **30**, 131 (1958).
20. G. Kloosterman, "Contact methods in finite element simulations," PhD thesis, Univ. of Twente (2002).
21. M. Brunet, *Numiform'92 Proc.* Chenot, Wood, and Zienkiewicz, Eds., Balkema, Rotterdam, 1992.

Biographies and photographs of authors not available.